



Manganese oxide-based catalysts for toluene oxidation



Z. Sihaib^{a,b}, F. Puleo^b, J.M. Garcia-Vargas^a, L. Retaillieu^a, C. Descorme^a, L.F. Liotta^b, J.L. Valverde^c, S. Gil^{a,*}, A. Giroir-Fendler^{a,*}

^a Univ Lyon, Université Claude Bernard Lyon 1, CNRS, IRCELYON, 2 avenue Albert Einstein, Villeurbanne F-69622, France

^b Istituto per lo Studio dei Materiali Nanostrutturati (ISMN)-CNR, via Ugo La Malfa, 153, 90146 Palermo, Italy

^c Facultad de Ciencias y Tecnologías Químicas, Departamento de Ingeniería Química, Universidad de Castilla-La Mancha, 13071 Ciudad Real, Spain

ARTICLE INFO

Article history:

Received 14 January 2017

Received in revised form 11 March 2017

Accepted 15 March 2017

Available online 19 March 2017

Keywords:

Perovskite

OMS

Manganese Oxide

Oxidation

Toluene

ABSTRACT

Four different catalysts based on manganese oxide were prepared: a perovskite (LaMnO_3), via sol-gel method; Mn_2O_3 , rapid method and an Octahedral Molecular Sieve (OMS-2) by two different preparation methods, via solid state (OMS_s) and hydrothermal method (OMS_h). The physicochemical properties of these catalysts were characterized by X-ray diffraction (XRD), N_2 adsorption-desorption at -196°C , thermogravimetric and differential thermal analysis (TGA/DTA), inductively coupled plasma optical emission spectroscopy (ICP-OES) and temperature-programmed reduction with hydrogen (H_2 -TPR). Their catalytic performances were evaluated in the catalytic oxidation of toluene. Three consecutive catalytic cycles were performed for each catalyst in order to reach steady state performances. In order to assess the stability of the catalysts under reaction conditions, the catalytic performances were studied upon long term experiments running for 24 h at 25% of toluene conversion. For comparison purposes, the catalytic activity of the present manganese oxide catalysts was compared with that of typical industrial catalysts such as a commercial $\text{Pd}/\text{Al}_2\text{O}_3$ catalyst containing 0.78% Pd. The crystalline features detected in the XRD patterns, are well-consistent with the formation of the desired structures. Based on their specific surface area and their low-temperature reducibility, the catalysts were ranked as follows: $\text{OMS}_s > \text{Mn}_2\text{O}_3 > \text{OMS}_h > \text{LaMnO}_3$. This trend was in good agreement with the performances observed in the catalytic removal of toluene. A kinetic model was proposed and a good agreement was obtained upon fitting with the experimental data.

© 2017 Elsevier B.V. All rights reserved.

1. Introduction

Volatile Organic Compounds (VOCs) emitted from industrial processes and automobile are not only harmful to human health because they are malodorous, mutagenic and/or carcinogenic but also because they can form toxic photochemical oxidants and suspended particulate matters through photochemical reactions. Many countries have already enacted stringent legislations to abate VOC emissions [1].

In order to efficiently remove VOCs, various technologies have been developed, including adsorption, bio-degradation, membrane separation, thermal incineration and photo-catalytic oxidation [2]. Among these technologies, catalytic oxidation is considered as the most promising process for limiting VOCs' emissions. Indeed, catalytic oxidation might be operated at temperatures much lower compared to thermal incineration. The advantage of the low

temperature oxidation is the reduction of fuel consumption, particularly for large volumes of diluted VOC contaminated air. The optimization of the catalyst formulation is not an easy task due to the large variety of VOCs and the complexity of VOC-containing mixtures. Primarily, the catalyst has to allow ignition temperatures as low as possible. Moreover, it has to be very active, due to the low concentration of VOCs and the large volumes to be treated, and also highly selective in the sense that only CO_2 and H_2O should be produced. Finally, the catalyst has to withstand the reaction conditions over long periods of operation, i.e., has to be thermally stable.

Noble metal catalysts demonstrated higher activity compared to base metal catalysts; however, their cost is much higher. Therefore, many efforts are being paid to the development of transition metal oxide-based catalysts with high catalytic activity. Among them, manganese oxide-based catalysts are the most active ones [3,4]; although such oxides usually exhibit low specific surface area and poor thermal stability. An interesting way to obtain new manganese oxide-based structures (LaMnO_3 , OMS and Mn_2O_3), with smaller crystallite size (i.e. higher specific surface area) and

* Corresponding authors.

E-mail addresses: sonia.gil@ircelyon.univ-lyon1.fr, soniagilvillarino@gmail.com (S. Gil), anne.giroir-fendler@ircelyon.univ-lyon1.fr (A. Giroir-Fendler).

improved stability, is the implementation of new preparation methods.

As one of the possible substitutes for precious metal catalysts in redox processes, perovskite-type metal oxides, more specifically LaMnO₃-based perovskites, have attracted much attention due to their adequate catalytic activity and good thermal stability in the catalytic oxidation of various hydrocarbons. For example, Spinicci et al. [5] investigated the catalytic combustion of acetone, isopropanol and benzene over LaMnO₃ perovskites. The presence of surface oxygen species, easily available and sufficiently mobile, was proposed as a fundamental requirement for the high catalytic activity of LaMnO₃. Alvarez-Galvan et al. [6] have studied the combustion of methyl ketone over La-transition metal (Cr, Co, Ni, Mn) perovskites. The LaMnO₃ catalyst exhibited the best catalytic performances with complete methyl ketone conversion being achieved at 297 °C. However, in order to ascertain the formation of the perovskite structure, calcination of the precursor material at high temperature (typically above 600 °C) is necessary, leading to relatively low specific surface area and poor reducibility at low temperature in comparison with other transition metal oxides. Therefore, in order to obtain perovskites with high specific surface area and outstanding redox ability, selection and optimization of the synthesis method is a key parameter. For example, the sol-gel method was earlier shown to yield well-crystallized samples with larger specific areas [7].

In addition, OMS-2 is a type of manganese oxide with edge and corner-shared MnO₆ octahedra, forming a 2 × 2 tunnel structure, with K⁺ ions inside the tunnel for charge compensation. Because of its unique structural characteristics, OMS-2 has been extensively investigated for various applications in thermocatalytic oxidations such as the chemical synthesis or the cleanup of organic pollutants [8,9]. The activity of OMS-2 catalysts was tentatively attributed to their physicochemical properties, such as their specific surface area, their morphology and/or their surface acidity [10,11].

Similarly, cryptomelane-type of OMS was used in the catalytic oxidation of a variety of VOCs; namely, benzene [12,13], toluene [14], ethanol [10,15] and ethyl acetate [10]. The high activity of such catalysts was alternatively attributed to the presence of the redox Mn(III)/Mn(IV) couple, the high mobility of lattice oxygen, the open structure of cryptomelanes and/or the high hydrophobicity of these solids. Ding et al. [16] used a solvent-free method (solid state method) to synthesize cryptomelane-type of catalysts and investigated the possible correlation between the specific surface area of the catalysts and their catalytic performances. The results showed that the catalysts with the highest surface area (95 m² g⁻¹) exhibited the best catalytic performances in the oxidation of toluene. The same trend was observed when OMS-2 was synthesized using the hydrothermal method. The best performances in the oxidation of toluene also corresponded to higher surface area, higher reducibility and/or higher mesopore diameter.

Finally, it is reported in the literature that manganese oxide catalysts, such as Mn₂O₃, exhibit high performances in the catalytic oxidation of VOCs. The most active manganese oxide catalysts were those with the best redox properties and the highest oxygen mobility [16,17]. Various methods have been used to prepare Mn₂O₃, such as co-precipitation, hydrothermal process, sol-gel method and microwave synthesis. However, the gas-liquid reaction method (referred as rapid preparation method in the following) was shown to be the most appropriate since it is simple, easy to control, low-cost and fast [18]. Moreover, large surface area solids could be obtained.

In the present study, Mn catalysts have been prepared using different procedures. All catalysts were characterized by BET, XRD, TGA-DTA, H₂-TPR and ICP-OES and evaluated in the catalytic oxidation of toluene, chosen as target VOC molecule.

2. Experimental

2.1. Catalyst preparation

Based on the state-of-the-art, different synthesis routes were selected for the preparation of different families of Mn oxide catalysts. The sol-gel method was the most appropriate for perovskites (LaMnO₃) [2], the solid state route for OMS_s [19], the hydrothermal synthesis for OMS_h [16] and the rapid preparation method for Mn₂O₃ (Mn₂O_{3R}) [20].

2.1.1. LaMnO₃ (Sol-gel method)

Nitrates (La(NO₃)₃·6H₂O, Fluka, 99 wt.% and Mn(NO₃)₂·4H₂O, Alfa Aesar, 98 wt%) were used as metal precursors to prepare the LaMnO₃ perovskite-type oxides. Equimolar amounts of the nitrates were weighed and mixed in a beaker. Distilled water was used to prepare the aqueous nitrates solution. Citric acid (CA) was purchased from Alfa Aesar (>99.5 vol%). The CA to total metal ions (La³⁺ + Mn²⁺) molar ratio was fixed at 1.5. After CA addition, the solution was heated up to 80 °C under magnetic stirring to evaporate the excess water. The preparation was dried at 120 °C overnight and subsequently treated in a muffle furnace at 200 °C (2 °C min⁻¹) for 1 h. Finally, the solid was calcined at 750 °C (5 °C min⁻¹) for 2 h in a quartz tubular reactor under static air.

2.1.2. OMS_s (Solid state method)

9.48 g of KMnO₄ (Sigma-Aldrich, 99.0 wt%), and 22.05 g Mn(Ac)₂·4H₂O (Sigma-Aldrich, 99.0 wt%) were homogeneously grounded in an agate mortar. The powder was further introduced in a capped glass bottle and maintained at 80 °C for 4 h. A black powder was received. After washing with deionized water, the solid was dried at 100 °C for 12 h. Then, the resulting material was calcined at 500 °C (5 °C min⁻¹) for 2 h in a quartz tubular reactor under static air.

2.1.3. OMS_h (Hydrothermal method)

0.04 mol (6.76 g) of MnSO₄·H₂O (Sigma-Aldrich, 99.0 wt%) was dissolved in 40 mL of water. The pH of the solution was adjusted to 1.0 using concentrated HNO₃ (Sigma-Aldrich, 90 vol%). An aqueous permanganate solution, prepared by dissolving 0.028 mol (4.40 g) of KMnO₄ (Sigma-Aldrich, 99.0 wt%) in 150 mL of water, was then slowly added to the previous solution under vigorous stirring. The pH of the mixture was again adjusted to 1.0. The mixture was subsequently transferred in a glass liner and sealed in a stainless steel autoclave.

The autoclave was placed in an oven and maintained at 100 °C for 16 h. After cooling, the received black precipitate was filtered and then washed thoroughly with water. The sample was finally dried at 120 °C for 16 h and calcined at 500 °C (5 °C min⁻¹) for 2 h in a quartz tubular reactor under static air.

2.1.4. Mn₂O₃ (Rapid preparation method)

4.9018 g (20 mmol) of Mn(CH₃COO)₂·4H₂O (Sigma-Aldrich, 99.0 wt%) was dissolved in 100 mL of ethanol. After addition of 40 mL NH₃·H₂O (Sigma-Aldrich, 25.0 vol%), the solution, from colourless turned to light red. However, no precipitate was formed. Subsequently, 1.5 L min⁻¹ air was bubbled into the solution for 5 min at 50 °C. The solution gradually changed to deep black as colloids were formed. These colloids appeared to be evenly dispersed in the bulk of the solution and stable. Finally, the suspension was centrifuged, dried at 110 °C over night and calcined at 500 °C (the heating rate of 5 °C min⁻¹) for 2 h in a quartz tubular reactor under air atmosphere.

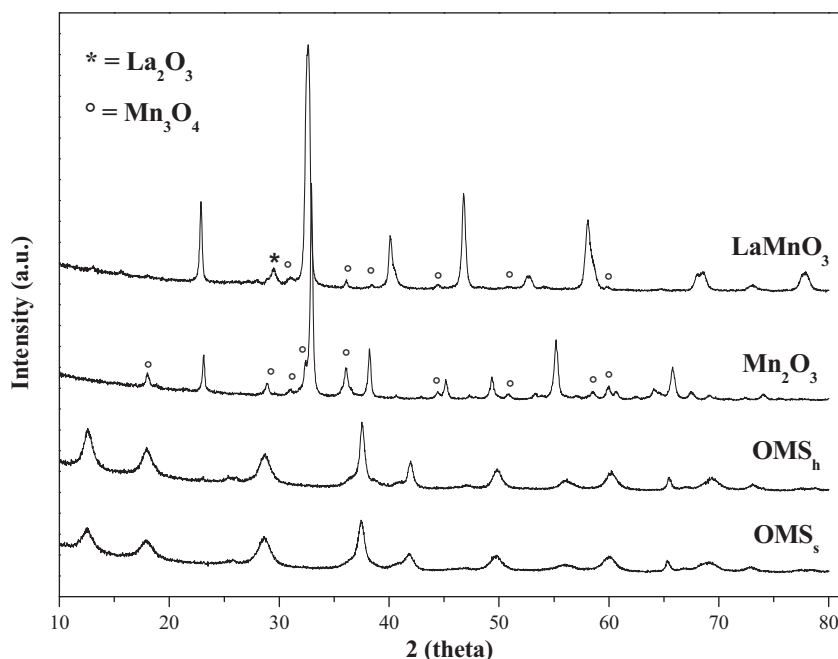


Fig. 1. XRD patterns of catalysts LaMnO₃, Mn₂O₃, OMS_h and OMS_s.

2.2. Catalysts characterization

Powder X-ray diffraction (XRD) patterns were recorded on a Bruker D5005 diffractometer equipped with a Cu K α radiation ($\lambda = 1.5418 \text{ \AA}$) and a graphite monochromator on the diffracted beam. Unless clearly stated, XRD patterns were collected in the 2-theta range 10–80° with a step size of 0.05°. The crystallite size (d_{XRD}) was further calculated according to the Debye-Scherrer equation.

Nitrogen adsorption-desorption isotherms at -196°C were obtained using a Micromeritics Tristar 3000 surface area and porosity analyzer. Before measurement, the samples were outgassed at 300°C for 3 h under primary vacuum. The specific surface area (SSA) of each sample was obtained using the Brunauer–Emmett–Teller (BET) method. The porous volume and the pore size distribution were calculated using the Barrett–Joyner–Halenda (BJH) method.

The catalyst composition was assessed by inductively coupled plasma optical emission spectroscopy, ICP-OES (Horiba Jobin Yvon).

Thermogravimetric and differential thermal analysis (TGA/DTA) were carried out over the dried catalysts (non-calcined catalysts) in the temperature range 25–900°C ($10^\circ\text{C min}^{-1}$) on a SETARAM Setsys Evolution 12 calorimeter, using 2–7 mg of sample, under flowing air.

Temperature-programmed reduction (TPR) experiments were performed in a commercial BELCAT-B unit with TCD detection. Samples (ca. 0.1 g) were loaded into a U-shaped quartz tube and pre-treated at 250°C for 30 min under Ar flow ($50 \text{ cm}^3 \text{ min}^{-1}$). After cooling down, the temperature was ramped from room temperature to 900°C ($10^\circ\text{C min}^{-1}$), using a reducing gas mixture consisting of 5 vol.% H₂ in Ar ($50 \text{ cm}^3 \text{ min}^{-1}$). H₂ uptakes upon TPR experiments were calculated as follows:

$$H_2 \text{ uptake} = \frac{\text{mmol}_{H_2 \text{ consumed}}}{\text{mmol}_{Mn}} \quad (1)$$

The average oxidation state of Mn was calculated from the total consumption of hydrogen upon TPR experiments (total H₂-uptake), considering the overall Mn loading in the catalysts and assuming that the final oxidation state of Mn was +2.

2.3. Toluene catalytic oxidation

2.3.1. Experimental setup

Catalytic testing was carried out using 100 mg of catalyst mixed with silicon carbide (SiC) to avoid any hot spot. The catalyst was immobilized over a quartz wool plug in a U-shaped reactor. The reactive mixture, containing 1000 ppm C₇H₈ and synthetic air (80/20 vol%) with a total flow of 100 mL min^{-1} , was introduced over the catalyst at room temperature before heating at a ramp rate of 5°C min^{-1} up to 100°C for 30 min, in order to stabilize the system. Subsequently, a second temperature ramp of 2°C min^{-1} was applied up to 400°C . After such a treatment, all catalysts were tested upon cooling the reactor down to room temperature. This sequence was repeated three times. Reproducible results were systematically obtained upon successive toluene oxidation runs. Moreover, the catalytic performance of the catalysts were evaluated upon long term toluene oxidation test, running for 24 h at 25% of toluene conversion, to evaluate the catalysts stability. The overall toluene conversion ($X_{\text{C}_7\text{H}_8}$) was defined as follows:

$$X_{\text{C}_7\text{H}_8} (\%) = 100 \cdot \frac{[\text{C}_7\text{H}_8]_{\text{in}} - [\text{C}_7\text{H}_8]_{\text{out}}}{[\text{C}_7\text{H}_8]_{\text{in}}} \quad (2)$$

Where $[\text{C}_7\text{H}_8]_{\text{in}}$ and $[\text{C}_7\text{H}_8]_{\text{out}}$ are the inlet and outlet concentrations of toluene, respectively.

In order to compare the activity of our catalysts with a commercial one in the same experimental conditions, a Pd/Al₂O₃ catalyst containing 0.78% Pd was also evaluated in the toluene combustion during 3 cycles. This catalyst was calcined in air at 450°C prior to reaction, where 64.1 mg of sample were diluted with SiC keeping the same gas hourly space velocity than in the rest of experiments.

2.3.2. Analysis of the reaction products

Toluene and the possible organic products were analyzed using a gas chromatograph (GPC, PERKIN ELMER Clarus-500) equipped with both a flame ionization detector (FID) and thermal conductivity detector (TCD) and using a capillary column (Chromosorb 101) for the organic reaction intermediates and a packing column (Carboxen 1000) for the permanent gas, respectively. In addition, CO and CO₂ were continuously measured on-line by IR (ROSE-

Table 1
Physicochemical properties of the catalysts.

Catalyst	Pretreatment	SSA ^a (m ² g ⁻¹)	pore volume (cm ³ g ⁻¹)	D _p ^b (nm)	Mn(wt.%)	d _{XRD} ^c (nm)	H ₂ -uptake (mmol _{H₂} mmol _{Mn} ⁻¹) ^d			Mn average oxidation state ^d
							200–600 °C	700–900 °C	Total	
LaMnO ₃	750 °C 2 h in air	6	0.046	18	21.6	42.1	0.23	0.33	0.56	3.1
Mn ₂ O ₃	500 °C 2 h in air	37	0.20	18	69.6	38.3	0.42	–	0.42	2.8
OMS _h	500 °C 2 h in air	71	0.69	35	52.2	21.3	0.85	0.25	1.10	4.2
OMS _s	500 °C 2 h in air	95	0.25	12	55.3	23.7	0.65	–	0.65	3.3

^a SSA: Specific surface area.

^b D_p: pore diameter.

^c d_{XRD}: Crystallite size.

^d Calculated from the TPR experiments.

MOUNT Xstream analyzer). No other organic hydrocarbon was ever detected among the reaction products.

3. Results and discussion

3.1. XRD characterization

XRD patterns were acquired after calcination of the catalysts at 500 °C, except in the case of LaMnO₃ which required a higher calcination temperature for the crystallization of the perovskite structure (750 °C). The XRD patterns are shown in Fig. 1. The crystallite sizes (d_{XRD}), calculated according to the Debye-Scherrer equation, are listed in Table 1 along with other physicochemical properties.

The crystal structure of each sample was deduced by comparison with the standard powder diffraction files (PDF) from the International Centre for Diffraction Data (ICDD).

The diffraction lines of the LaMnO₃ sample were in good accordance with those of the reference La_{0.951}Mn_{0.951}O₃ (PDF 89-8775) with rhombohedral symmetry (space group R-3c). Diffraction line at 2θ = 28.98° was assigned to the presence of La₂O₃ (PDF 5-602). Moreover, diffraction peaks assignable to Mn₃O₄ (PDF 2-1062) were also detected. Comparing with previous results [2], the perovskite structure and phase purity seem to depend on the synthesis conditions, such as on the citric acid to total metal ions molar ratio.

The XRD pattern for Mn₂O₃ was also in good agreement with the reference Mn₂O₃ sample (PDF 04-008-6383) with cubic symmetry. Characteristic diffraction lines of Mn₃O₄ were also present.

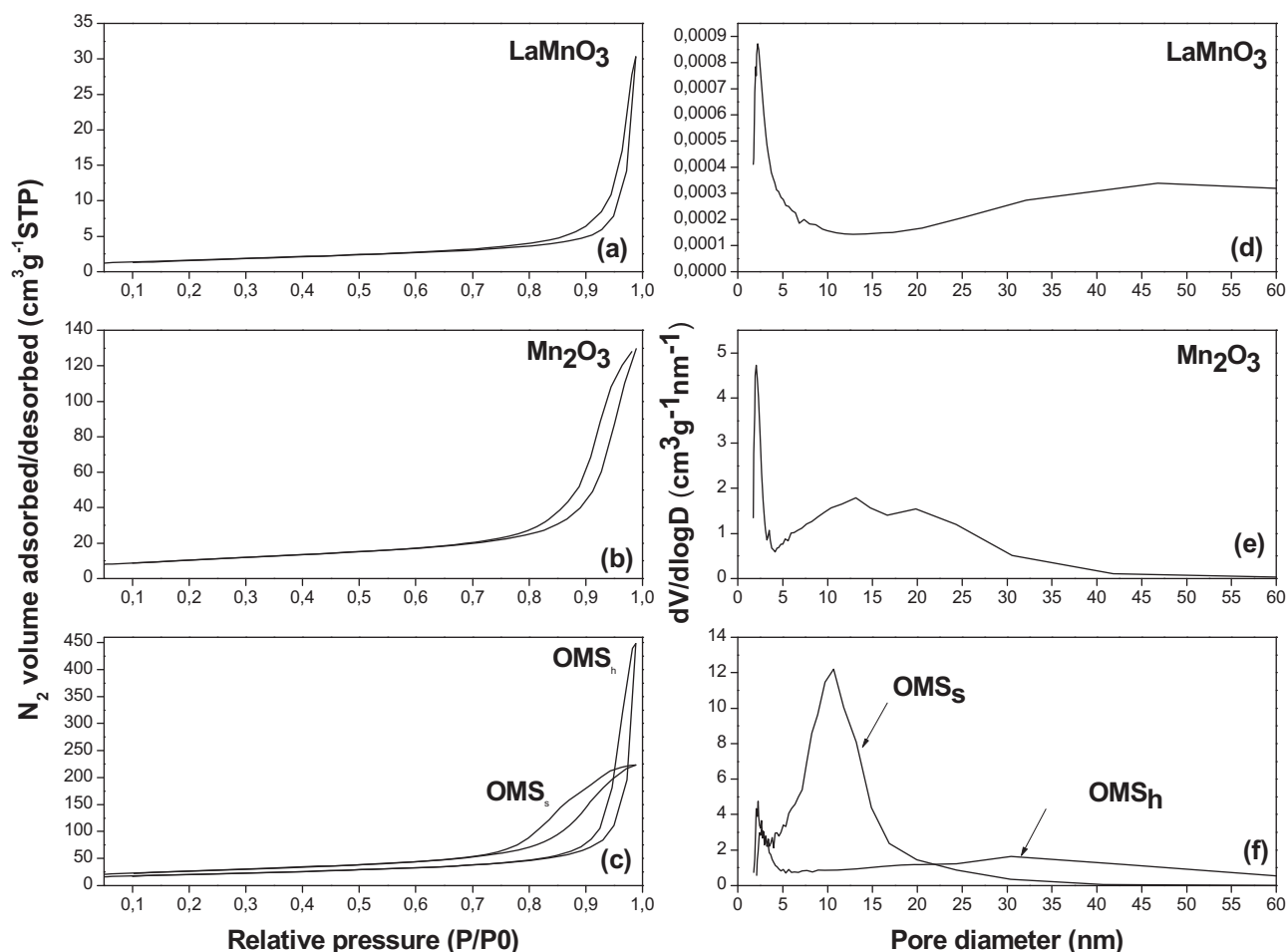


Fig. 2. (a), (b) and (c) N₂ adsorption–desorption isotherms and (d), (e) and (f) pore-size distributions of catalysts.

The OMS_h structure corresponded to K_{0.34}Mn₄O₈ (PDF 04-017-1191) with a tetragonal symmetry, whereas the OMS_s structure corresponded to KMn₈O₁₆ (PDF 00-012-0706), with tetragonal symmetry.

3.2. N₂ adsorption-desorption (at –196 °C)

N₂ adsorption-desorption isotherms and pore size distributions of the so far prepared catalysts are presented on Fig. 2. The specific surface areas and pore volumes are summarized in Table 1. As observed from Fig. 2, the N₂ adsorption-desorption isotherms were all characteristic of a mixed microporous and mesoporous structures with H3-type of hysteresis [21,22]. Such mixed porous structure was also evidenced by the pore-size distributions on Fig. 2. While most pores were in the range 10–40 nm, additional micropores were systematically observed in minor amount in the range 1.0–4.0 nm.

As shown in Table 1, OMS_s exhibited the largest specific surface area (95 m² g^{–1}) but not the highest pore volume (0.25 cm³ g^{–1}). OMS_h had a lower SSA (71 m² g^{–1}) but the highest pore volume (0.69 cm³ g^{–1}). The physicochemical properties of the OMS catalysts, such as the specific surface area and the porous texture, appeared to be directly influenced by the preparation method. Mn₂O₃ showed intermediate SSA and pore volume (37 m² g^{–1} and 0.20 cm³ g^{–1}, respectively). Finally, LaMnO₃ had the lowest SSA and pore volume (6 m² g^{–1} and 0.046 cm³ g^{–1}, respectively). However, one must take into consideration that LaMnO₃ was calcined at 750 °C instead of 500 °C.

3.3. Thermogravimetric and differential thermal analysis

The thermal stability and crystallization of the prepared samples were studied using TGA/DTA analyses that were carried out under air in the temperature range 25–900 °C on the dried catalysts (still containing the organic precursors). The results are presented in Fig. 3.

In the case of the LaMnO₃ perovskite catalyst, the TG plot shows a first small weight loss (–5 wt%) around 115 °C, corresponding to the removal of residual water in the gel, accompanied by a small endothermic peak in the DTA profile. Subsequently, a sharp exothermic peak with a concurrent pronounced weight loss of ca. 41% was registered at 290 °C, indicating that the decomposition of nitrate ions and citric acid contained in the gel occurred suddenly, in a single step, with the production of large amounts of gas such as H₂O, CO₂ and NO_x [23]. The second small exothermic peak observed at 470 °C with an additional weight loss (–60 wt% on the overall) might be attributed to the decomposition of unreacted citric acid. At around 700 °C, the crystallization of the perovskite structure occurs. Accordingly, a broadened exothermic peak is visible in the DTA with a further small weight loss. At the end, i.e. at 900 °C the overall weight loss was –64 wt%.

In the case of Mn₂O₃, after a preliminary small weight loss (–2 wt%) at around 140 °C, corresponding to the removal of residual water, a significant weight loss (–14%) due to the oxidation of the organic precursors was observed along with a sharp exothermic peak centered at 245 °C. Upon increasing the temperature, the Mn₃O₄ phase is oxidized to Mn₂O₃, with a small weight gain ca. 630 °C accompanied by a broad exothermic peak [24].

As it concerns the TGA plots of OMS_h and OMS_s, slightly different thermal stabilities were observed, with an overall weight loss of 11 and 13 wt%, respectively. For both samples, four different steps can be detected in the TG curves: a first step from 25 to ca. 200 °C where a weight loss (around 3–5.5 wt%) occurred. According to the literature [16,25–28], loss of the water physically adsorbed on the surface or in the porous structure of the molecular sieves took place. Subsequently, a weight loss (ca. 3 wt.%) was observed between 200

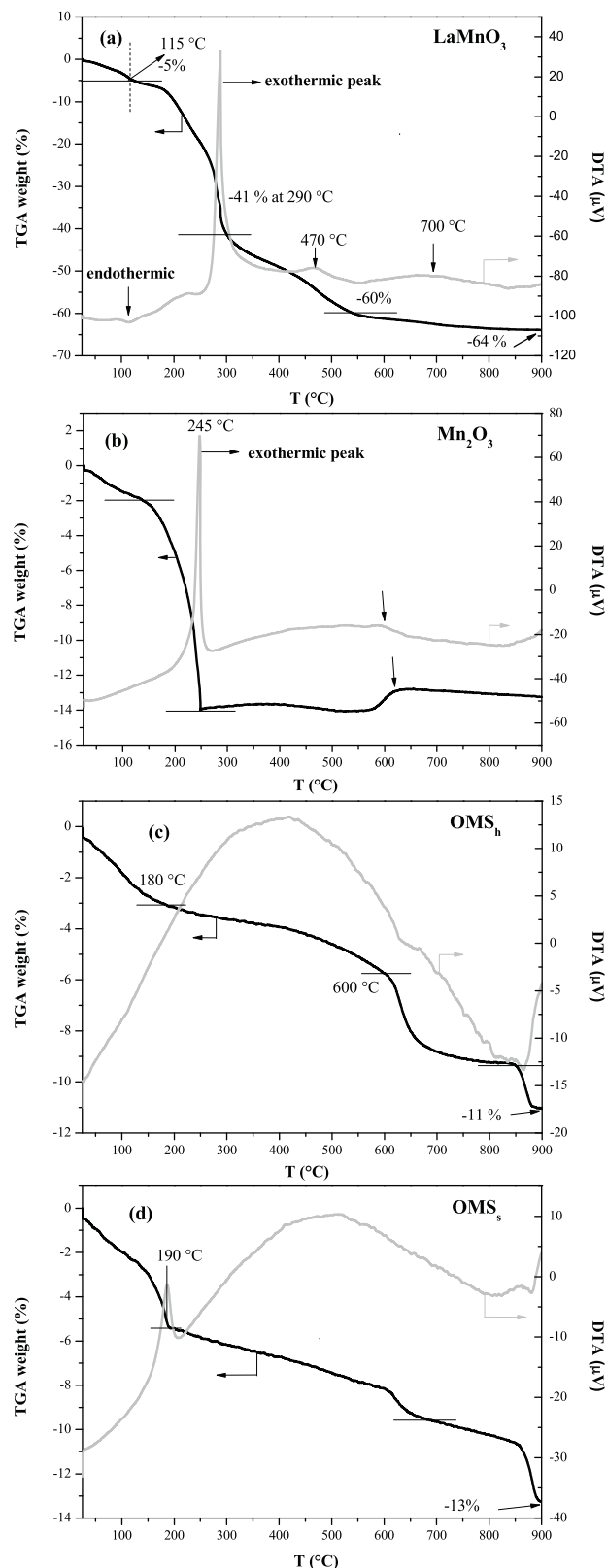


Fig. 3. DTA and TGA profiles received under air for all catalysts (a) LaMnO₃, (b) Mn₂O₃, (c) OMS_h and (d) OMS_s.

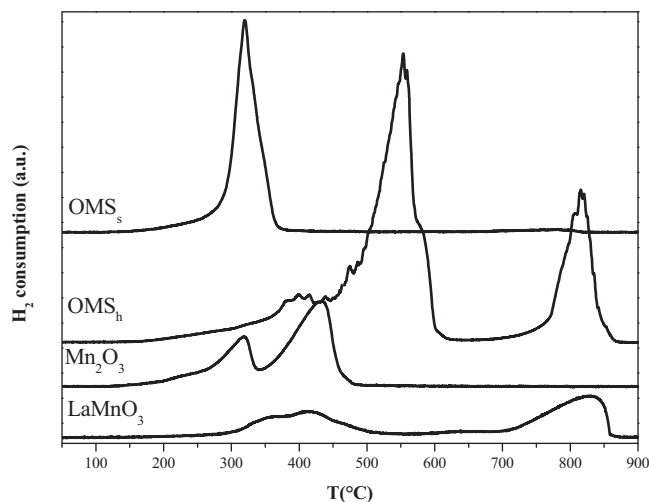


Fig. 4. H_2 -TPR profiles of samples $LaMnO_3$, Mn_2O_3 , OMS_h , OMS_s .

and 600 °C as a result of the release of chemically adsorbed water and of any organic residual precursors if still present [16,25]. At the end of such step crystallization of the OMS structure occurs. In a third step, between 600 and 700 °C, both OMS samples lost ca. 3 and 1.4 wt% for OMS_h and OMS_s , respectively. This could be due to the evolution of the lattice oxygen species and the transformation of the OMS structure to Mn_2O_3 [25,28]. Above 800 °C (fourth step) due to a further oxygen release (weight loss of 1.7 and 2.5 wt% for OMS_h and OMS_s , respectively), transformation to Mn_3O_4 took place [25,28]. The so far discussed weight losses are accompanied by broad exothermic peaks in the temperature range 200–800 °C.

3.4. H_2 -TPR

In order to investigate the relative reducibility of the samples, H_2 -TPR experiments were conducted. H_2 -TPR profiles are shown on Fig. 4. The corresponding H_2 consumptions are summarized in Table 1. It could be observed that all catalysts showed two overlapping reduction peaks, except OMS_s , corresponding to a two-step reduction process. The first one occurred in the temperature range 200–600 °C, while the second one occurred at higher temperature, above 700 °C. In the case of Mn_2O_3 both peaks appeared below 600 °C.

The reduction profile registered for the $LaMnO_3$ perovskite catalyst was in good agreement with our previous results [2], both in terms of reduction temperatures and H_2 consumptions. A first broad peak centered on 400 °C was observed, with a small shoulder ca. 360 °C. The later contribution, at the lowest temperature, was attributed to the removal of surface oxygen species [2,29]. At higher temperature, a larger H_2 consumption appeared, with a maximum centered around 414 °C, corresponding to the reduction of Mn^{4+} to Mn^{3+} . The H_2 consumption in the temperature range 200–600 °C was $0.23 \text{ mmol}_{H_2} \text{ mmol}_{Mn}^{-1}$ (Table 1). However, by increasing the temperature even further, an intense peak

centered around 828 °C was noticed, related to the subsequent reduction of Mn^{3+} into Mn^{2+} [2,29]. The H_2 -uptake at high temperature ($0.33 \text{ mmol}_{H_2} \text{ mmol}_{Mn}^{-1}$) was even higher than the one registered ca. 400 °C (reduction of Mn^{4+} to Mn^{3+}), indicating that two oxidation states of Mn (Mn^{4+} and Mn^{3+}) coexisted in the initial catalyst.

For the Mn_2O_3 nanocrystals, two peaks centered around 320 and 440 °C were observed, corresponding to a stepwise reduction process from Mn_2O_3 to Mn_3O_4 and MnO [30].

H_2 -TPR profiles for the two prepared OMS showed clear differences depending on the preparation method. Assuming that MnO was the final reduction state [19], in the case of sample OMS_h , the first reduction peak at low temperature was assigned to the reduction of MnO_2/Mn_2O_3 to Mn_3O_4 . The second peak ca. 800 °C, with an H_2 -uptake of $0.253 \text{ mmol}_{H_2} \text{ mmol}_{Mn}^{-1}$, was attributed to the reduction of Mn_3O_4 to MnO [17,19]. The reduction profile of the OMS_s sample consisted of one single peak, around 300 °C, which appeared at a lower temperature than that observed for OMS_h . Similar results were reported for an OMS sample prepared by sol-gel method in the presence of maleic acid and methoxypolyethylene glycol [31]. From the comparison between the two OMS samples, it was concluded that the Mn species in OMS_s were more reducible at low temperatures compared to OMS_h . Nevertheless, the total H_2 consumption was higher in the case of OMS_h compared to OMS_s , indicating that the average oxidation state of Mn was higher for OMS_h (Table 1). As observed in Table 1, the preparation method had a great influence on the initial oxidation state of Mn. OMS_s showed the highest proportion of Mn^{3+} with respect to Mn^{4+} (average oxidation state: ca. 3.3), while in the case of OMS_h , Mn^{4+} was predominant (average oxidation state ca. 4.2).

3.5. Catalytic performances in the catalytic oxidation of toluene

Catalytic activity measurements were performed as light-off experiments. The catalysts stability was further assessed upon consecutive light-off runs.

In details, the catalyst stability was firstly evaluated by performing three consecutive catalytic runs for each catalyst. The conversion-temperature profiles (light-off curves) obtained upon three consecutive cycles, during the cooling ramp, are shown on Fig. 5. The results obtained upon the second catalytic run for all catalysts are shown in Fig. 6. Temperatures for achieving 10, 50 or 90% toluene conversion are listed in Table 2. These values were used to compare the catalysts performance. All samples showed a limited decrease in the T_{50} values of about 12 °C after three cycles (Table 2). Complete conversion of toluene could be successfully achieved below 350 °C for all catalysts. The final products of the reaction were CO_2 and H_2O . No other by-product was ever detected. The prepared catalysts ranked as follows: $OMS_s > Mn_2O_3 > OMS_h > LaMnO_3$. OMS_s exhibited the best catalytic activity in the toluene oxidation with T_{10} , T_{50} and T_{90} values of 195, 234 and 272 °C, respectively. Indeed, OMS_s also exhibited the highest specific surface area and an optimum reducibility at low temperature. On the contrary, $LaMnO_3$ logically demonstrated

Table 2

Catalytic performances of the catalysts in the oxidation of toluene. Data were collected upon cooling.

Catalysts	1 st Run			2nd Run			3rd Run		
	$T_{10} \text{ } ^\circ\text{C}^1$	$T_{50} \text{ } ^\circ\text{C}^1$	$T_{90} \text{ } ^\circ\text{C}^1$	$T_{10} \text{ } ^\circ\text{C}^1$	$T_{50} \text{ } ^\circ\text{C}^1$	$T_{90} \text{ } ^\circ\text{C}^1$	$T_{10} \text{ } ^\circ\text{C}^1$	$T_{50} \text{ } ^\circ\text{C}^1$	$T_{90} \text{ } ^\circ\text{C}^1$
$LaMnO_3$	244	283	320	250	289	326	256	295	332
Mn_2O_3	233	256	274	240	266	292	244	266	282
OMS_h	213	257	311	219	267	330	224	271	336
OMS_s	188	227	263	195	234	272	202	240	276

¹Light-off temperature at 10, 50 and 90% toluene conversion, respectively.

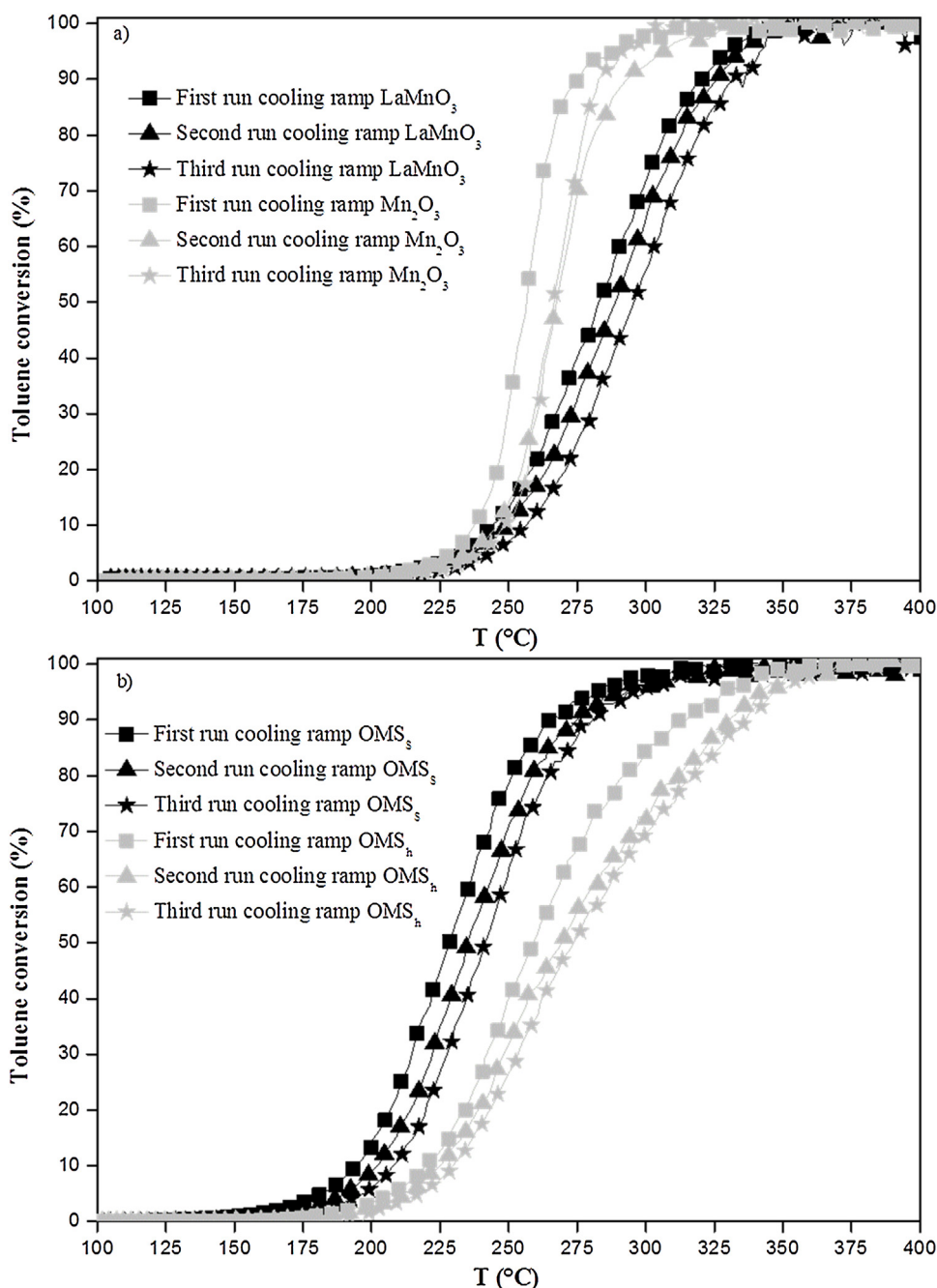


Fig. 5. Evolution of the toluene conversion as a function of temperature, while cooling the reactor, upon three consecutive runs (a) LaMnO₃ and Mn₂O₃, and (b) OMS_s and OMS_h.

the lowest catalytic performances since it exhibited the poorest reducibility at low-temperature and the lowest SSA.

Moreover, it could be observed that OMS_s performed better than OMS_h. Total toluene conversion into CO₂ was achieved at 300 °C over OMS_s; while only 73% conversion was achieved over OMS_h at the same temperature. Comparing the specific surface areas of both OMS catalysts, one could conclude that the specific surface area had only a minor impact on the catalytic activity. In fact, toluene has a kinetic diameter of 5.8 Å, while the OMS structures exhibit pore dimensions ca. 4.6 × 4.6 Å. Therefore, catalytic oxidation of toluene obviously occurs on the external surface of OMS. This could be the reason why the surface area would only have a minor influence. On the opposite, OMS_s clearly appeared to be more reducible than OMS_h, especially at low temperature. It has

been pointed out in different studies that the catalytic oxidation of toluene followed a Mars-Van Krevelen-type of mechanism when using transition metal oxide catalysts [32,33]. As such, the reaction mechanism involved several redox steps, including the oxidation of toluene with surface oxygen species, the reduction of the oxidized catalyst by toluene, and the oxidation of the catalyst by oxygen to form surface oxygen species again. For that, the ability of the catalyst to shift between different oxidation states at the lowest possible temperature is expected to improve the catalytic performances. In conclusion, the solid state method is to be preferred for the synthesis of highly active OMS-based catalysts. Commercial Pd/Al₂O₃ showed a good conversion with a T₅₀ value slightly lower than the one of OMS_s. However, prepared OMS_s was more active at

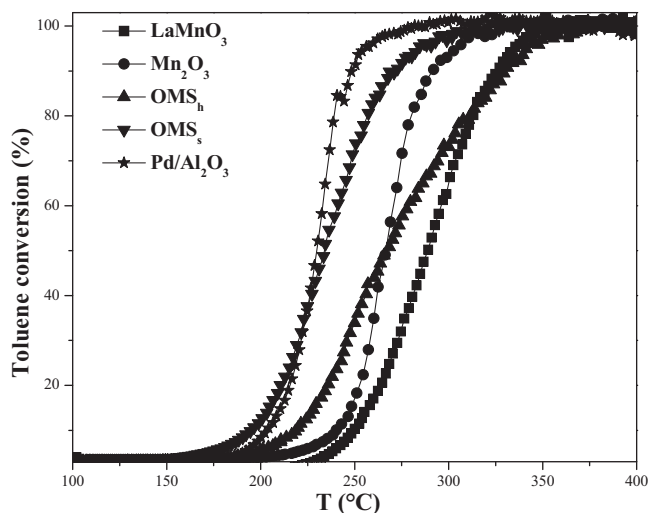


Fig. 6. Toluene conversion versus temperature during second consecutive run (cooling ramp).

low temperature, starting to convert toluene at about 170 °C while in the case of Pd/Al₂O₃ conversion started at about 190 °C.

The catalytic stability and durability of the catalysts were also evaluated under steady-state conditions at 25% of toluene conversion after the first run. Fig. 7 illustrates toluene conversion as a function of time on stream (24 h) for all catalysts. LaMnO₃ and OMS_s catalysts exhibited relative good catalytic stability and durability, with only a slight decrease in toluene conversion during the first 6 h (from 25% to 23%). However, Mn₂O₃ and OMS_h catalysts were deactivated most quickly during this 6 h, at which point 21 and 15% of toluene conversion, respectively were noted.

A comparison between the data already reported in the literature and the results obtained in the present study in the catalytic oxidation of toluene is proposed in Table 3. The performances of different Mn-containing catalysts, including one commercial Pd/Al₂O₃ catalyst, are summarized in this table. Our results are comparable to those already reported in the literature for the dif-

ferent Mn-containing catalysts. OMS_s appeared as the most active ones.

4. Kinetic study

A kinetic study of the toluene oxidation was performed by using 100 mg of catalyst placed over a quartz wool plug in a U-shaped reactor. The reactive mixture, containing 1000 ppm C₇H₈ and synthetic air (80/20 vol.%) with a total flow of 100 mL min⁻¹ was introduced over the catalyst at room temperature before heating at ramp rate of 5 °C min⁻¹ up to 100 °C for 30 min to stabilize the system. Subsequently, a second temperature ramp of 2 °C min⁻¹ was applied up to 400 °C. Toluene conversion was calculated by Eq. (2). The following reaction was considered:



Experimental catalytic activity of the C₇H₈ transformation was defined by the experimental reaction rate, r_{Exp} , expressed as mol s⁻¹ g⁻¹ of Mn (Eq. (4)):

$$r_{\text{exp}} = \frac{Q_v \cdot \left(\frac{P_{T0} - P_T}{P} \right) \cdot \left(\frac{1}{T \cdot R} \right)}{m_{\text{Mn}}} \quad (4)$$

Where Q_v is the total flow of the gas stream L s⁻¹; P_T is the partial pressure of toluene; P_{T0} is the partial pressure of toluene (in atm); P is the total pressure in the reactor (1 atm); T is the temperature at which the volume flow was measured (298 K); R is the ideal gas constant (0.082 atm L K⁻¹ mol⁻¹); and m_{Mn} is the mass in grams of Mn in the catalyst bed used.

Experimental kinetic data obtained for catalysts LaMnO₃, Mn₂O₃, OMS_h and OMS_s in the oxidation of toluene were used for evaluating the parameters of the power-law rate, r_{Th} , represented by Eq. (5): pre-exponential factor of the kinetic constant, the activation energy and the partial order of reactions [42,43]:

$$r_{\text{Th}} = k' P_{\text{O}_2}^{n_{\text{O}_2}} P_{\text{Tol}}^{n_{\text{Tol}}} \quad (5)$$

Since the partial pressure of O₂ was in excess respect to that of toluene, this equation could be simplified to the next one:

$$r_{\text{Th}} = k P_{\text{Tol}}^{n_{\text{Tol}}} \quad (6)$$

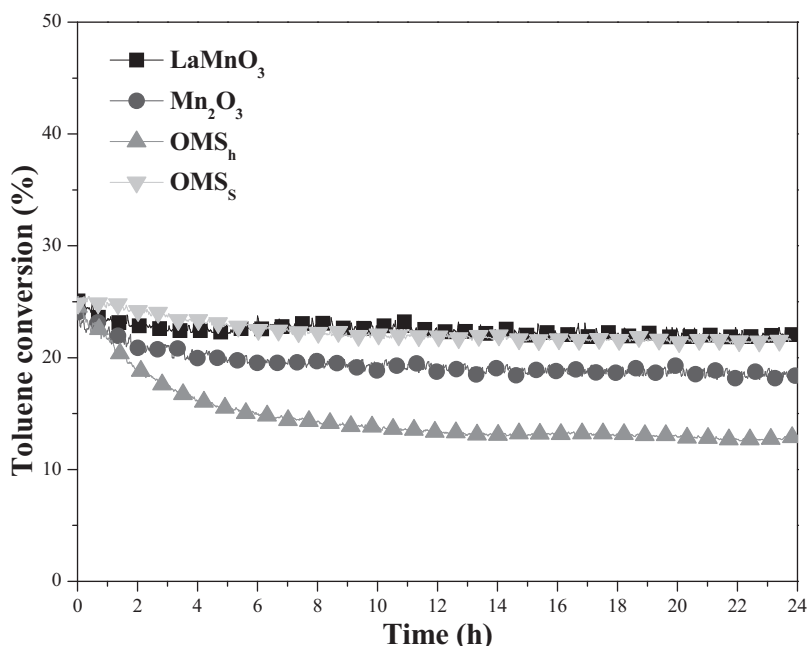


Fig. 7. Lifetime toluene oxidation test conducted at 25% of toluene conversion during 24 h.

Table 3

Catalytic conversion for combustion of toluene reported in the literature.

Catalysts	Preparation Method	Oxidation conditions	Toluene conversion	Reference
LaMnO ₃	Citrate sol–gel	1000 ppm Toluene	T ₅₀ = 203 °C	[2]
	Glycine combustion	15000 mL g ⁻¹ h ⁻¹	T ₅₀ = 239 °C	
	Co-precipitation		T ₅₀ = 213 °C	
LaMnO ₃	Citrate sol–gel	1000 ppm Toluene	T ₅₀ = 358 °C	[34]
		60000 mL g ⁻¹ h ⁻¹		
OMS-2	Refluxing	1000 ppm Toluene	T ₅₀ = 215 °C	[19]
	solid-state reaction	20000 h ⁻¹	T ₅₀ = 270 °C	
Mn ₂ O ₃	PMMA-templating strategy	1000 ppm Toluene	T ₅₀ = 268 °C	[35]
		20000 mL g ⁻¹ h ⁻¹		
Mn ₂ O ₃	solution combustion synthesis	1000 ppm Toluene	T ₅₀ = 245 °C	[36]
		19100 h ⁻¹		
5%Mn _x O _y /Al ₂ O ₃	Incipient wetness	4000 ppm Toluene	T ₅₀ = 335 °C	[37]
	impregnation	3600 mL g ⁻¹ h ⁻¹		
30%Mn _x O _y /Al ₂ O ₃	Impregnation	1000 ppm Toluene	T ₅₀ = 340 °C	[38]
60%Mn _x O _y /Al ₂ O ₃		200000 mL g ⁻¹ h ⁻¹	T ₅₀ = 290 °C	
Mn _x O _y /TiO ₂	Impregnation	1000 ppm Toluene	T ₅₀ = 315 °C	[39]
		35000 h ⁻¹		
15%Mn _x O _y /Al ₂ O ₃	Incipient wetness	1000 ppm Toluene	T ₅₀ = 300 °C	[40]
	impregnation	4800 h ⁻¹		
Pd/Al ₂ O ₃	Impregnation	1000 ppm Toluene	T ₅₀ = 179 °C	[41]
		60000 mL g ⁻¹ h ⁻¹		
LaMnO ₃	Citrate sol–gel	1000 ppm Toluene	T ₅₀ = 289 °C	This work
		60000 mL g ⁻¹ h ⁻¹		
OMS-2	solid-state reaction	1000 ppm Toluene	T ₅₀ = 234 °C	This work
	Hydrothermal	60000 mL g ⁻¹ h ⁻¹	T ₅₀ = 267 °C	
Mn ₂ O ₃	Rapid preparation	1000 ppm Toluene	T ₅₀ = 266 °C	This work
		60000 mL g ⁻¹ h ⁻¹		

Where $k = k' P_{O_2}^{n_{O_2}}$; P_{Tol} is the partial pressure of toluene; and n_{Tol} is the partial order of reaction (toluene). The apparent rate constant (k) was considered to be temperature dependent according to the Arrhenius equation:

$$k = k_0 \exp\left(\frac{-E_a}{RT}\right) \quad (7)$$

Where E_a is the activation energy (J mol⁻¹); R is the gas constant (J mol⁻¹ K⁻¹); k_0 is the pre-exponential factor; and T is the reaction temperature (K).

The tubular flow reactor with a packed catalyst bed that was used in this work was modelled with a pseudo homogeneous, one-dimensional model. Isothermal conditions and no pressure drops were assumed. Therefore, the following expression for the axial flow profiles through the reactor for the fed gases can be used:

$$\frac{dF_T}{dm_{Mn}} = -r_{Th} \quad (8)$$

where F_T represents the flow-rate of toluene in any point of the fixed bed.

A VBA-Excel application was developed to solve this model [44,45]. The Bader-Deufhard method was used in the evaluation of the set of ordinary differential equations [45], whereas the Marquard-Levenberg algorithm was used in the nonlinear regression procedure [44,46]. The weighted sum of the squared differences between the observed and the calculated outlet flow rates was minimized [45]:

$$SSQ = \sum_i (F_{T,exp} - F_{T,th})^2 \quad (9)$$

where SSQ is the sum of square differences; $F_{T,exp}$ and $F_{T,t}$ denote the experimental and theoretical molar effluent of toluene, respectively.

An F-test is a statistical test in which the test statistic has an F-distribution under the null hypothesis. It was used for comparing statistical models that have been fitted to a data set, in order to identify the model that best fits the population from which the data were sampled. The procedure was based on the comparison

between the tabulated F value (F-test) and F_c , which is defined by the following Eq. [44]:

$$F_c = \frac{\text{regression sum of squares/degree of freedom}}{\text{residual sum of squares/degrees of freedom}} = \frac{\sum_{i=1}^N \{[f(x, \beta)]^2 / p\}}{\sum_{i=1}^N \{[y - f(x, \beta)]^2 / (N - P)\}} \quad (10)$$

Note that if $F_c > F(p, N-p, 1-\alpha)$ (assuming a value of $\alpha = 0.05$, 95% confidence level), the regression is considered to be meaningful, although there is no guarantee that the model is statistically suitable. To avoid this contradiction, the meaningfulness of the parameters in the model must also be evaluated by using the t -test, which verifies whether the estimation of β_i (b_{fi}) differs from a reference value (generally zero). Thus, a parameter will be always meaningful when the following inequality can be achieved:

$$t_{ci} = \frac{|b_{fi}|}{\sqrt{[V(b_f)]_{ii}}} > t(N-p; 1 - \frac{\alpha}{2}) \quad (11)$$

Where $[V(b_f)]_{ii}$ represents the diagonal j th term of the covariance matrix. Finally, the confidence interval of the parameter β_i is defined by:

$$b_{fi} - t(N-p; 1 - \frac{\alpha}{2}) \sqrt{[V(b_f)]_{ii}} \leq \beta_j \leq b_{fi} + t \times (N-p; 1 - \frac{\alpha}{2}) \sqrt{[V(b_f)]_{ii}} \quad (12)$$

Where F_c : function defined by Eq. (10); t_{ci} : function defined by Eq. (11); b : estimate of β ; $V(b)$ covariance matrix; N : total number of experiments; x : set of independent variables in $f(x, \beta)$ mode; y : experimental dependent variable; $f(x, \beta)$, mathematical model; p : number of parameters in a model; i : the species.

In all cases, the regressions were considered to be meaningful. Table 4 provides the corresponding model parameters and t -tests.

Comparison of SSQ values identifies Marquardt-Levenberg algorithm model. The t -test showed that the regression could be considered to be meaningful, because the value of the t_c/t_{test} ratio was greater than 1.

Table 4
Statistical meaningful of kinetic model parameters.

Catalyst	Parameters	Estimated values	t_c	t_{test}	t_c/t_{test}	Statistical significance
LaMnO ₃	ko (mol s ⁻¹ g Mn ⁻¹ bar ^{-nTol})	9.86E+08	4.11	1.96	2.1	Yes
	Ea (J mol ⁻¹)	123312	174.6	1.96	89.1	Yes
	n_{Tol}	1.45E+00	108.9	1.96	55.5	Yes
Mn ₂ O ₃	ko (mol s ⁻¹ g Mn ⁻¹ bar ^{-nTol})	1.90E+08	3.036	1.96	1.55	Yes
	Ea (J mol ⁻¹)	133680	184.5	1.96	94.13	Yes
	n_{Tol}	9.3E-01	27	1.96	13.77	Yes
OMS _h	ko (mol s ⁻¹ g Mn ⁻¹ bar ^{-nTol})	3.70E+11	2.187	1.96	1.11	Yes
	Ea (J mol ⁻¹)	126520	104.4	1.96	53.26	Yes
	n_{Tol}	1.9E+00	78.12	1.96	39.85	Yes
OMS _s	ko (mol s ⁻¹ g Mn ⁻¹ bar ^{-nTol})	8.80E+07	1.15	1.96	0.58	Not
	Ea (J mol ⁻¹)	96920	45.12	1.96	23	Yes
	n_{Tol}	1.9E+00	34.4	1.96	17.55	Yes

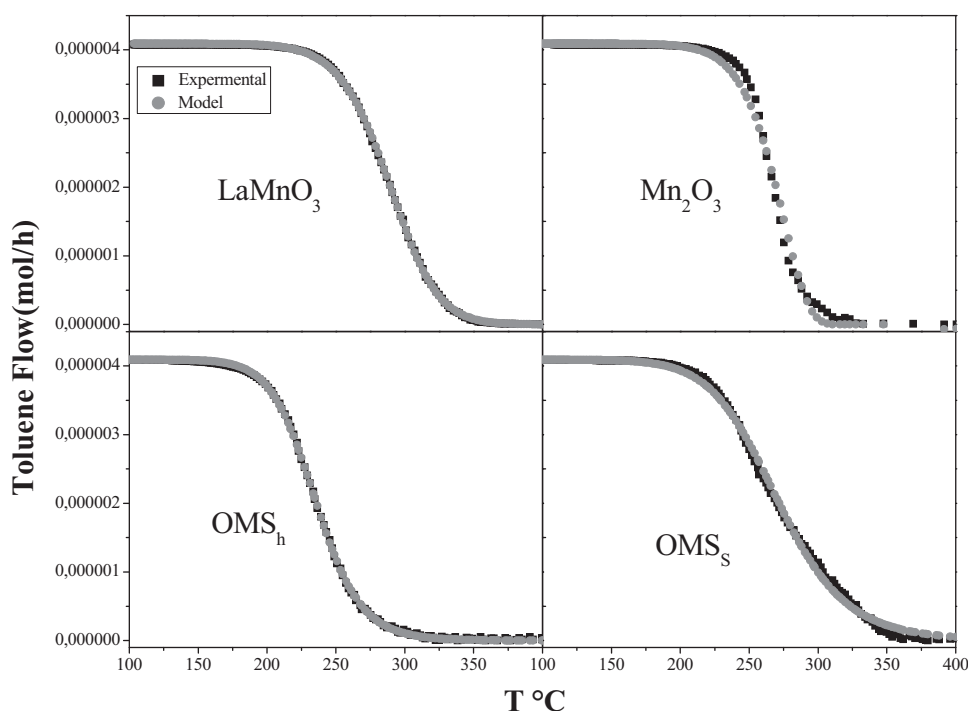


Fig. 8. Comparison between experimental and predicted toluene molar flow for catalysts LaMnO₃, Mn₂O₃, OMS_h and OMS_s.

Although the power law model is only mathematical and is not directly connected to the reaction mechanism, its simplicity allows a preliminary approach to obtain kinetic values similar to those reported in literature [47] and it easy to be implemented into commercial software (like Aspen HYSYS, ASPEN Plus or UNISIM) which would allow one to develop more engineering studies based on the computation of the thermodynamic efficiencies, energy analysis and LCA.

As observed, the toluene partial orders of reaction ranges from 0.9 and 1.9 which means that the effect of the concentration of toluene is directly related to the kind of catalyst used and could indicate that the mechanism of reaction over the different catalysts could not be the same. Further studies should be done in order to elucidate this finding. On the other hand, different activation energies ranging from 96.9 kJ mol⁻¹ to 133.6 kJ mol⁻¹ have been estimated. Behar et al. [47] have recently review the values of the activation energies of the total oxidation of toluene over different catalysts. According to them, values of activation energy ranging from 42 to 145 kJ mol⁻¹ should be expected which are in good agreement with those reported in this work. Finally, the higher value of the pre-exponential factor for catalyst OMS_h should be

directly related as seen in Fig. 8 to its higher catalytic activity if compared to that of the rest of catalysts.

In Fig. 8 the experimental and predicted molar flow of toluene for all the catalysts tested are represented. It can be observed an excellent good agreement between the experimental and predicted data even at high temperatures. This result and the fact that high values of the activation energies were estimated by nonlinear regression for all the catalysts would clearly indicate that the reaction is the only rate-limiting step.

5. Conclusions

Four different catalysts based on manganese oxide (LaMnO₃, OMS and Mn₂O₃) were prepared using several preparation routes. For the synthesis of OMS two different preparation routes, solid state (OMS_s) and hydrothermal method, were employed. The OMS_s catalyst, prepared via solid state method, exhibited the highest catalytic activity for the complete oxidation of toluene at low temperature, which could be related to its higher reducibility and higher specific surface area. The catalytic performances of the catalysts followed the order: OMS_s > OMS_h > Mn₂O₃ > LaMnO₃. In all

cases the reaction started at around 200–250 °C with full conversion of toluene being achieved below 350 °C. This trend was in agreement with the trend in the evolution of the specific surface area. Also, the loading (wt%) of the active element of the catalysts (Mn) followed a similar trend than the catalytic activities except for Mn_2O_3 , which is the one with the highest loading of Mn but its surface area is lower than half of the surface area of the catalyst with the highest catalytic activity (OMS_5). All catalysts demonstrated to be stable upon three consecutive runs. A comparison between the present results with the performances of different Mn-containing catalysts, already reported in the literature, show comparable activity with our systems, OMS_5 being the most active one. Tests of toluene oxidation over a commercial $\text{Pd}/\text{Al}_2\text{O}_3$ catalyst were also performed for comparison purposes. Although for such Pd catalyst a T_{50} value slightly lower than the one of OMS_5 was found, the OMS_5 was more active at low temperature. A kinetic study was carried out and a model was developed with an excellent good agreement between the experimental and predicted data even at high temperatures. For all the catalysts, the reaction is the only rate-limiting step.

Acknowledgements

This work was financially supported by the Libyan Ministry, Université Lyon 1 and CNRS (PICs program PROXIVOC 2015–2017). The contribution of the joint Ph.D. Program between the Libyan Scholarship Council, the Institute de recherches sur la catalyse et l'environnement de Lyon (IRCELYON), University Claude Bernard Lyon 1 (UCBL1), the Istituto per lo Studio dei Materiali Nanostrutturati (ISMN) of Palermo and the University of Castilla La Mancha, Spain is also acknowledged.

References

- [1] M. Popova, A. Szegedi, Z. Cherkezova-Zhelva, I. Mitov, N. Kostova, T. Tsoncheva, Toluene oxidation on titanium- and iron-modified MCM-41 materials, *J. Hazard. Mater.* 168 (2009) 226–232.
- [2] C. Zhang, Y. Guo, A. Boreave, L. Retailleau, A. Baylet, A. Giroir-Fendler, LaMnO_3 perovskite oxides prepared by different methods for catalytic oxidation of toluene, *Appl. Catal. B: Environ.* 148–149 (2014) 490–498.
- [3] A. Gil, L.M. Gandia, S.A.A. Korili, Effect of the temperature of calcination on the catalytic performance of manganese- and samarium-based oxides in the complete oxidation of acetone, *Appl. Catal. A* 274 (1) (2004) 229–235.
- [4] T.A. Mellan, K.P. Maenettja, P.E. Ngoepe, S.M. Woodley, C.R.A. Catlow, R.J. Grau-Crespo, Lithium and oxygen adsorption at the $\beta\text{-MnO}_2$ (110) surface, *J. Mater. Chem.* 1 (2013) 14879–14887.
- [5] R. Spinicci, M. Faticanti, P. Marini, S. De Rossi, P. Porta, Catalytic activity of LaMnO_3 and LaCoO_3 perovskites towards VOCs oxidation, *J. Mol. Catal. A: Chem.* 197 (2003) 147–155.
- [6] M.C. Alvarez-Galvan, V.A. de la Peña O'shea, G. Arzamendi, B. Pawelec, L.M. Gandia, J.L.G. Fierro, Methyl ethyl ketone combustion over La-transition metal (Cr, Co, Ni, Mn) perovskites, *Appl. Catal. B: Environ.* 92 (2009) 445–453.
- [7] M.A. Peña, J.L.G. Fierro, Chemical structures and performance of perovskite oxides, *Chem. Rev.* 101 (2001) 1981–2017.
- [8] S.L. Suib, Porous manganese oxide octahedral molecular sieves and octahedral layered materials, *Acc. Chem. Res.* 41 (4) (2008) 479–487.
- [9] V.P. Santos, O.S.G.P. Soares, J.J.W. Bakker, M.F.R. Pereira, J.J.M. Orfao, J. Gascon, F. Kapteijn, J.L. Figueiredo, Structural and chemical disorder of cryptomelane promoted by alkali doping: influence on catalytic properties, *J. Catal.* 293 (2012) 165–174.
- [10] A.R. Gandhe, J.S. Rebelló, J.L. Figueiredo, J.B. Fernandes, Manganese oxide OMS_2 as an effective catalyst for total oxidation of ethyl acetate, *Appl. Catal. B: Environ.* 72 (1) (2007) 129–135.
- [11] V.D. Makwana, Y.C. Son, A.R. Howell, S.L. Suib, The role of lattice oxygen in selective benzyl alcohol oxidation using OMS_2 catalyst: a kinetic and isotope-labeling study, *J. Catal.* 210 (2002) 46–52.
- [12] J. Luo, Q. Zhang, A. Huang, S.L. Suib, Microporous and Mesoporous Materials, *Mat.* 35–36 (2000) 209–217.
- [13] J. Luo, Q. Zhang, J. Garcia-Martinez, S.L. Suib, Adsorptive and acidic properties reversible lattice oxygen evolution, and catalytic mechanism of cryptomelane-type manganese oxides as oxidation catalysts, *J. Am. Chem. Soc.* 130 (2008) 3198–3207.
- [14] M.I. Dominguez, P. Navarro, F. Romero-Sarria, D. Frias, S.A. Cruz, J.J. Delgado, M.A. Centeno, M. Montes, J.A. Odriozola, Fibrous MnO_2 nanoparticles with (2×2) tunnel structures. catalytic activity in the total oxidation of volatile organic compounds, *J. Nanosci. Nanotechnol.* 9 (6) (2009) 3837–3842.
- [15] M.A. Peluso, E. Proncato, J.E. Sambeth, H.J. Thomas, G. Busca, Catalytic oxidation of ethanol on pure and alumina supported K-Mn oxides: an IR and flow reactor study, *Appl. Catal. B: Environ.* 78 (1) (2008) 73–79.
- [16] Y.S. Ding, X. Shen, S. Sithambaram, S. Gomez, R. Kumar, M.B. Vincent, S.L. Suib, Synthesis and catalytic activity of cryptomelane-type manganese dioxide nanomaterials produced by a novel solvent-free method, *Chem. Mater.* 17 (21) (2005) 5382–5389.
- [17] H. Sun, Z. Liu, S. Chen, X. Quan, The role of lattice oxygen on the activity and selectivity of the OMS_2 catalyst for the total oxidation of toluene, *Chem. Eng. J.* 270 (2015) 58–65.
- [18] B. Chen, G. Rao, S. Wang, Y. Lan, L. Pan, X. Zhang, Facile synthesis and characterization of Mn_3O_4 nanoparticles by auto-oxidation method, *Mater. Lett.* 154 (2015) 160–162.
- [19] H. Sun, S. Chen, P. Wang, X. Quan, Catalytic oxidation of toluene over manganese oxide octahedral molecular sieves (OMS_2) synthesized by different methods, *Chem. Eng. J.* 178 (2011) 191–196.
- [20] X.L. Cui, Y.L. Li, S.Y. Li, G.C. Sun, J.X. Ma, L. Zhang, T.M. Li, R.B. Ma, Mn_3O_4 nano-sized crystals: rapid synthesis and extension to preparation of nanosized LiMn_2O_4 materials, *J. Chem. Sci.* 126 (2014) 561–567.
- [21] X. Wang, X. Zhang, Y. Wang, H. Liu, J. Qiu, J. Wang, W. Han, K.L. Yeung, Investigating the role of zeolite nanocrystal seeds in the synthesis of mesoporous catalysts with zeolite wall structure, *Chem. Mater.* 23 (20) (2011) 4469–4479.
- [22] B. Pawelec, V. La Parola, R.M. Navarro, S. Murcia-Mascaros, J.L.G. Fierro, On the origin of the high performance of MWNT-supported PtPd catalysts for the hydrogenation of aromatics, *Carbon* 44 (1) (2006) 84–98.
- [23] A. Mali, A. Ataie, Structural characterization of nano-crystalline $\text{BaFe}_{12}\text{O}_{19}$ powders synthesized by sol-gel oxidation route, *Scr. Mater.* 53 (9) (2005) 1065–1070.
- [24] D. Larcher, G. Sudant, R. Patrice, J.M. Tarascon, Some insights on the use of polyols-based metal alkoxides powders as precursors for tailored metal-oxides particles, *Chem. Mater.* 15 (15) (2003) 3543–3551.
- [25] F. Schurz, J.M. Baucher, T. Merker, T. Schleid, H. Hasse, R. Glaser, Octahedral molecular sieves of the type K- OMS_2 with different particle sizes and morphologies: impact on the catalytic properties in the aerobic partial oxidation of benzyl alcohol, *Appl. Catal. A: Gen.* 355 (1) (2009) 42–49.
- [26] X. Chen, Y.F. Shen, S.L. Suib, C.L. O'Young, Characterization of manganese oxide octahedral molecular sieve (M- OMS_2) materials with different metal cation dopants, *Chem. Mater.* 14 (14) (2002) 940–948.
- [27] H. Huang, Y. Meng, A. Labonte, A. Doble, S.L. Suib, Large-Scale synthesis of silver manganese oxide nanofibers and their oxygen reduction properties, *J. Phys. Chem. C* 117 (48) (2013) 25352–25359.
- [28] J. Luo, Q.H. Zhang, J. Garcia-Martinez, S.L. Suib, Adsorptive and acidic properties, reversible lattice oxygen evolution, and catalytic mechanism of cryptomelane-type manganese oxides as oxidation catalysts, *J. Am. Chem. Soc.* 130 (10) (2008) 3198–3207.
- [29] H. Najjar, J.F. Lamoniér, O. Mentré, J.M. Giraudon, H. Batis, Optimization of the combustion synthesis towards efficient LaMnO_{3+y} catalysts in methane oxidation, *Appl. Catal. B: Environ.* 106 (2011) 149–159.
- [30] V. Iablokov, K. Frey, O. Geszti, N. Kruse, High catalytic activity in CO oxidation over MnO_x nanocrystals, *Catal. Lett.* 134 (3–4) (2010) 210–216.
- [31] Y.U. Lin, S.U.N. Ming, Y.U. Jian, Y.U. Qian, H.A.O. Zhifeng, L.L. Chaosheng, Synthesis and characterization of manganese oxide octahedral molecular sieve and its catalytic performance for DME oxidation, *Chin. J. Catal.* 29 (11) (2008) 1127–1132.
- [32] P. Liu, H. He, G. Wei, D. Liu, X. Liang, T. Chen, J. Zhu, R. Zhu, An efficient catalyst of manganese supported on diatomite for toluene oxidation: manganese species, catalytic performance, and structure-activity relationship, *Microporous Mesoporous Mater.* 239 (2017) 101–110.
- [33] C. Doornkamp, V. Ponc, The universal character of the Mars and Van Krevelen mechanism, *J. Mol. Catal. A: Chem.* 162 (2000) 19–32.
- [34] A. Giroir-Fendler, M. Alves-Fortunato, M. Richard, C. Wang, J.A. Díaz, S. Gil, C. Zhang, F. Can, N. Bion, Y. Guo, Synthesis of oxide supported LaMnO_3 perovskites to enhance yields in toluene combustion, *Appl. Catal. B: Environ.* 180 (2016) 29–37.
- [35] Y. Liu, H. Dai, J. Deng, L. Zhang, Z. Zhao, X. Li, Y. Wang, S. Xie, H. Yang, G. Guo, Controlled generation of uniform spherical LaMnO_3 , LaCoO_3 , Mn_2O_3 , and Co_3O_4 nanoparticles and their high catalytic performance for carbon monoxide and toluene oxidation, *Inorg. Chem.* 52 (15) (2013) 8665–8676.
- [36] M. Piumetti, D. Fino, N. Russo, Mesoporous manganese oxides prepared by solution combustion synthesis as catalysts for the total oxidation of VOCs, *Appl. Catal. B: Environ.* 163 (2015) 277–287.
- [37] C.H. Wang, Al_2O_3 -supported transition-metal oxide catalysts for catalytic incineration of toluene, *Chemosphere* 55 (1) (2004) 11–17.
- [38] S.M. Sager, D.I. Kondarides, X.E. Verykios, Catalytic oxidation of toluene over binary mixtures of copper, manganese and cerium oxides supported on $\gamma\text{-Al}_2\text{O}_3$, *Appl. Catal. B: Environ.* 103 (3) (2011) 275–286.
- [39] P.O. Larsson, A. Andersson, L.R.B. Wallenberg, Svensson, Combustion of CO and toluene; characterisation of copper oxide supported on titania and activity comparisons with supported cobalt, iron, and manganese oxide, *J. Catal.* 163 (1996) 279–293.
- [40] S.C. Kim, The catalytic oxidation of aromatic hydrocarbons over supported metal oxide, *J. Hazard. Mater.* 91 (2002) 285–299.

- [41] J. Brunet, E. Genty, Y. Landkocz, M. Al Zallouha, S. Billet, D. Courcot, R. Cousin, Identification of by-products issued from the catalytic oxidation of toluene by chemical and biological methods *Comp. Rend. Chim.* 18 (2015) 1084–1093.
- [42] S. Behar, N.A. Gómez-Mendoza, M. Á. Gómez-García, D. Świerczyński, F. Quignard, N. Tanchoux, Study and modelling of kinetics of the oxidation of VOC catalyzed by nanosized Cu–Mn spinels prepared via an alginate route, *Appl. Catal. A: Gen.* 504 (2015) 203–210.
- [43] F. Duprat, Light-off curve of catalytic reaction and kinetics, *Chem. Eng. Sci.* 57 (6) (2002) 901–911.
- [44] S. Gil, M. Marchena, L. Sánchez-Silva, A. Romero, P. Sánchez, J.L. Valverde, Effect of the operation conditions on the selective oxidation of glycerol with catalysts based on Au supported on carbonaceous materials, *Chem. Eng. J.* 178 (2011) 423–435.
- [45] A.R. de la Osa, A. De Lucas, A. Romero, J.L. Valverde, P. Sánchez, Kinetic models discrimination for the high pressure WGS reaction over a commercial CoMo catalyst, *Int. J. Hydrogen Energy* 36 (2011) 9673–9684.
- [46] D.W. Marquardt, An algorithm for least squares estimation of nonlinear parameters, *J. Soc. Ind. Appl. Math.* 11 (1963) 431–441.
- [47] S. Behar, N.-A. Gómez-Mendoza, M.-A. Gómez-García, D. Świerczynski, F. Quignard, N. Tanchoux, Study and modelling of kinetics of the oxidation of VOC catalysed by nanosized Cu–Mn spinels prepared via an alginate route, *Appl. Catal. A* 504 (2015) 203–210.